Europium(III)/Terbium(III) mixed metal-organic frameworks and their application as a ratiometric thermometer

Madhura Joshi,[#,‡] Zhuang Wang,[♦,‡] Maurizio Riesner,[Δ,‡] Florian M. Wisser,[#] Rebecca Reber,[#] Marcus Fischer,[#] Rachel Fainblat,[Δ] Karl Mandel,[†] Doris Segets,[♦,] Gerd Bacher,[Δ,*] and Martin Hartmann[#,*]*

[#]Erlangen Center for Interface Research and Catalysis (ECRC), Friedrich-Alexander-Universität Erlangen-Nürnberg (FAU), Egerlandstraße 3 91058 Erlangen, Germany.

[Δ]Werkstoffe der Elektrotechnik and CENIDE, University of Duisburg-Essen, 47057 Duisburg, Germany

[♦]Particle Science and Technology, Institute of Combustion and Gas Dynamics – (IVG-PST), Carl-Benz-Straße 199, 47057 Duisburg, Germany

[†]Department of Chemistry and Pharmacy, Friedrich-Alexander-Universität Erlangen-Nürnberg, Egerlandstraße 1 91058 Erlangen, Germany

KEYWORDS: Eu Tb MOFs; BTC; photoluminescence spectra, temperature sensing

ABSTRACT The ability to molecularly engineer luminescent metal-organic frameworks is a powerful tool for the design of better performing rational temperature sensors. Lanthanide based MOF stand out as luminescent temperature sensors due to the high luminescence intensity and sharp emission lines of the lanthanides. The use of two different lanthanide cations incorporated into the same MOF

structure is supposed to allow for a rational, that is self-referencing, temperature sensing. Here, we present series of mixed $Eu_xTb_{(1-x)}BTC$, which were designed as nanoparticles. The $Eu_xTb_{(1-x)}BTC$ series shows controllable luminescent properties, which depend on the solvation of the lanthanide. The two MOFs in the series with the lowest Eu content, i.e. $Eu_{0.04}Tb_{0.96}BTC$ and $Eu_{0.02}Tb_{0.98}BTC$, are suitable candidates for rational temperature sensing in the range between 200 and 270 K and above 300 K.

Introduction

In the field of chemical sensing, metal-organic frameworks (MOF) have attracted much attention as they combine the advantages of high surface areas and pore volumes, crystallinity with tuneable structures and functionalities.[1,2] Thus, MOFs have found application in easy-to-read optical sensors,[3–5] as well as in electrochemical sensing[6,7] and fluorescent sensing.[1,8–11] As for other applications, MOF-based fluorescence sensors stands out compared to other materials due to their modular synthesis allowing to adjust the MOF structure and chemical composition and, thus, to tailor its properties. This has in the past allowed to design fluorescence sensors with high target selectivity as well as high sensitivities and low limit of detection. MOF-based fluorescence sensors have found application in various fields including toxic metal ion detections in wastewater, gas and volatile organic compounds detection but also for determination of physical properties such as pH value, humidity and temperature.[1,8–11]

To allow for ratiometric sensing, that is self-calibrating sensing without the use of an external reference, at least two different luminescent centres are required.[9] This can include two different metal complexes, e.g. two different lanthanides, two QDs or a combination of a QD and a metal complex. Lanthanide-based MOFs are attracting increasing attention due to the high luminescence intensity and sharp emission lines of the lanthanides.[11,12] Thus, from the two (or more) transitions originating from the different emissive centres within the same material, the sensor signal is determined optically as the ratio between the probe-dependent emission intensities. In case of temperature sensing, the nature of the MOF, i.e. the metal and organic linker combination, mainly

determine the temperature range which can be accurately measured. However, as ratiometric temperature sensing might offer large potential as an *in situ* probe to detect local temperature changes during a given application, e.g. a catalytic reaction or an adsorption process, precise understanding of the temperature sensing under different conditions is required. However, studies addressing this point are rare. This understanding is of significant importance, in particular as the luminescence in LnBTC's strongly depend on the conditions, e.g. the presence of a solvent.[13–15] It has been postulated that due to intermolecular interaction forces between the BTC linker – form the dispersed MOF – and the solvent, relaxation of excited BTC states occurs instead of energy transfer from excited BTC states to the luminescent Ln centers.[15]

Most of the pure Ln-containing MOFs known, show a preferred crystallization along one crystallographic direction leading typically to large needle-shaped crystals.[16–18] While this is very attractive for crystal structure determination, it may hamper their application in areas where size becomes important such as in contrasting agents in bio-imaging or in thin films. A prominent technique to control the size and shape of MOF crystals is the use of modulators. In their seminal report, Guo *et al.* reported the use of sodium acetate (NaOAc) as a suitable capping agent to reduce the particle size without affecting the crystal structure and properties of LnBTC MOFs.[19] While the original protocol allowed for the synthesis of rod-like LnBTC of several tenth of µm in length,[11,19] the protocol reported by Guo *et al.* lead to the synthesis of almost spherical particles with diameters below 100 nm. Those LnBTC (nano)particles have found wide application in the field of luminescent sensing, including small molecule detection,[13,20] and ratiometric temperature sensing[21] or in the field of luminescent thin films.[19,22,23]

Here we report the investigation of the ratiometric temperature sensing in a series of mixed europium and terbium BTC MOF, labelled as $Eu_xTb_{(1-x)}BTC$. Using the NaOAc-modulator approach, the $Eu_xTb_{(1-x)}BTC$ series was obtained as nanoparticular systems, to use them not only in the dry solid state but also dispersed in various solvents. Temperature sensing was established on dry powders of $Eu_{0.04}Tb_{0.96}BTC$ and $Eu_{0.02}Tb_{0.98}BTC$. Finally, we will show that an extension towards rational

temperature sensing in the presence of a solvent is feasible using the pure EuBTC and TbBTC as model compounds dispersed in ethanol.

Experimental Section

Materials and Methods

$Eu(NO_3)_3 \cdot 6H_2O$ (Thermo Scientific, 99.9%), $Tb(NO_3)_3 \cdot 6H_2O$ (Thermo Scientific, 99.99%), 1,3,5-benzene tricarboxylic acid (H_3BTC, Alfa Aeser, 98%), *N*,*N*-dimethylformamide (DMF, Merck, 99.5%), NaOAc (Merck, 99%) and ethanol (Merck, >95%). All chemicals were used as supplied without further purification.

Powder x-ray diffraction (PXRD) patterns were collected on a PANalytical Emryrean series 2 or on a PANalytical X'Pert Pro in Bragg-Brentano geometry using CuKα radiation at 2θ angles between 2 and 50°. Thermogravimetric analysis (TGA) of powder samples was measured on a Hi-Res TGA 2950 Thermogravimetric Analyzer (TA Instruments) in the temperature range from room temperature to 700 °C with a heating rate of 2 K/min in synthetic air. Inductively coupled plasma optical emission spectroscopy analysis was done using an SPECTRO Ciros-CCD. IR spectra were recorded using a JASCO FT/IR-4100 in attenuated total reflectance geometry (ATR, resolution 2 cm^{-1}, 64 scans), Photoluminescence (PL) spectra of the suspensions were recorded using a fluorescence spectrophotometer (Horiba Fluorolog) at 25 °C (room temperature) and 50 °C. PL spectra of the solid samples were recorded using a Jasco Spectrofluorometer FP-8500 (λ_{ex} = 256 nm). Scanning electron microscopy (SEM) images were obtained on a Carl Zeiss Gemini Ultra 55.

Synthesis procedure

Micrometer sized particles: The Ln-BTC MOF was synthesized following a modified literature procedure.[24] In a typical synthesis 670.0 mg (1.50 mmol) $Eu(NO_3)_3.6H_2O$ and 321.7 mg (1.50 mmol) H_3BTC were dissolved in a mixture of 45 ml DMF and 15 ml H_2O in a 100 ml Schott flask. The flask was

sealed and placed in an oven preheated to 80 °C. After 3 days, the reaction mixture was cooled to room temperature and the white needles formed were isolated by centrifugation, washed once with 30 ml DMF and the solvent exchanged with ethanol. After 1 h, the solid was isolated by centrifugation and the washing with ethanol repeated twice. The solid was dried at 80 °C over night to yield micro-EuBTC as white needles. Yield: 588 mg (1.22 mmol, 80 %).

Nanoparticulate $Eu_xTb_{(1-x)}$BTC MOFs: The MOF NPs were synthesized following a modified literature procedure.[19] In a typical synthesis of mixed LnBTC ($Eu_{0.5}Tb_{0.5}$BTC), 373.4 mg (4.5 mmol) NaOAc were dissolved in 57 ml DMF and 3 ml deionized H_2O in a 100 ml round bottom flask equipped with a reflux condenser. Next 339.8 mg (750 µmol) $Tb(NO_3)_3{\cdot}6H_2O$, 334.6 mg (750 µmol) $Eu(NO_3)_3{\cdot}6H_2O$ and 321.7 mg (1.5 mmol) H_3BTC were added and the synthesis mixture was heated to 110 °C and stirred at this temperature for 4 h (300 rpm). After cooling to room temperature, the white solid was isolated by centrifugation, washed with ca. 30 ml DMF and 30 ml absolute ethanol (three times). The white slurry was dried in an oven at 80 °C. Isolated yield: 471.3 mg (1.02 mmol, 68 %).

All $Eu_xTb_{(1-x)}$BTC NP samples were prepared following the procedure described above and are denoted accordingly to the experimentally determined molar ratios as: $Eu_xTb_{(1-x)}$BTC MOFs [x = 0 to 1].

Results and Discussion

Mixed-metal Eu/Tb BTC MOFs

The PXRD patterns of the as-synthesized LnBTC MOFs with varying ratios of Eu and Tb in the synthesis mixture ($Eu_xTb_{(1-x)}$BTC MOFs [x = 0.0 to 1.0]) are similar to each other and show the presence of characteristic peaks for the parent EuBTC[14] and [TbBTC]·(DMF)($H_2O_{0.5}$) (Figure 1a).[25] As the materials were obtained as nanoparticular powders (Figure 1e,f), they exhibit rather broad peaks. Thus, small changes in lattice parameters, expected when gradually replacing Eu with Tb, cannot be observed.

However, the very similar peak pattern and profiles observed confirm that a series of isostructural MOF is obtained. Here we note that the composition in the $Eu_xTb_{(1-x)}BTC$ has however an impact on the crystal shape. While the pure LnBTCs were obtained as spherical particles, the mixed-LnBTCs are still needle-shaped. The characteristic length of the particles, however, is always below 500 nm.

The thermal stability and decomposition behaviour of all materials is very similar as observed by thermogravimetric analysis (TGA) in air. Between room temperature and 275 °C desorption of remaining ethanol, water and/or DMF occur, while network decomposition only starts above 350 °C. The relative mass loss above 350 °C changes form approx. 49 % in case of EuBTC to approx. 47 % in case of TbBTC, in line with the expected values for the two pure phases. As final products of the decomposition Eu_2O_3 and Tb_4O_7 are obtained.[26] The results from TGA, combined with results from inductively coupled plasma optical emission spectroscopy (ICP OES), are thus indicative for an almost perfect one to one stoichiometry between lanthanides and BTC. Indeed, using ICP OES only traces of sodium are detected in all materials. The almost perfect stoichiometry is further evidenced by IR spectroscopy. The vanishing of the characteristic $\upsilon_{\mathrm{as}}(\mathrm{COO})$ vibration of H_3BTC around 1720 cm^{-1} in all MOFs of the series highlights that hardly any missing cluster defect is present (Figure 1c). Such a defect would give rise to only partially deprotonated H_3BTC which would in turn be characterised by its vibration around 1720 cm^{-1}. Likewise only traces of acetate might be present in this series of samples, as the characteristic CH vibrations around 2990 and 2930 cm^{-1} are barely visible. Interestingly, the accessibility towards nitrogen as probe molecule in physisorption experiments drops tremendously for the mixed metal MOFs in the series. While after activation at 150°C TbBTC shows an apparent surface area of 460 m^2/g, it drops to 170 m^2/g in EuBTC and below 100 m^2/g for the mixed metal LnBTCs. The apparent surface area of the pure MOFs are in line with literature reports on Tb and Eu MOFs,[20,25], but lower as compared to their Ho, Tm, Lu and Dy counterparts.[27] To the best of our knowledge no apparent surface area have been reported for similar mixed LnBTCs, albeit widely used.[12,19,22,23] Here we see, that the mixed LnBTCs possess significant lower apparent surface areas, the reason for this behaviour is yet not fully understood.

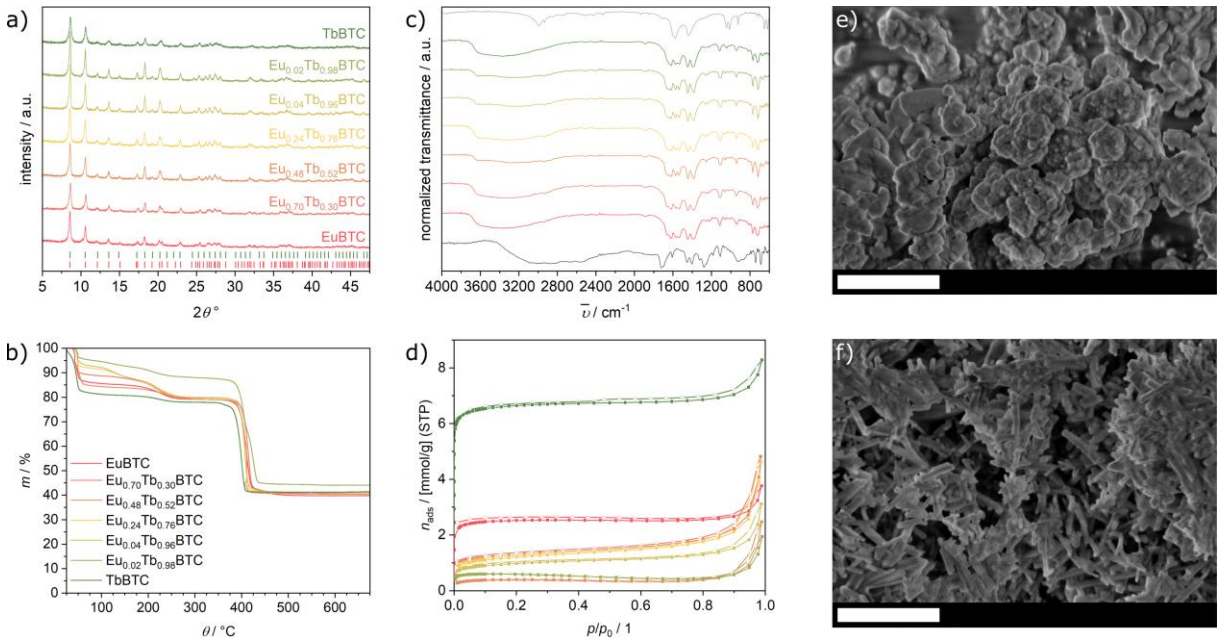

Figure 1. a) PXRD patterns of as-synthesized $Eu_xTb_{(1-x)}BTC$ MOFs [x = 0.0 to 1]. Bragg marker for [EuBTC (H_2O)]·$(H_2O)_{1.5}$ (red, CCDC 617492[14]) and [TbBTC]·$(DMF)(H_2O)_{0.5}$ (green[25]). b) TGA recorded under synthetic air (2K/min heating rate), c) IR spectra of $Eu_xTb_{(1-x)}BTC$ MOFs (same color code as in a) together with the IR spectrum of H_3BTC (dark grey) and NaOAc (light grey) and d) N_2 pysisorption isotherms recorded at 77 K (same color code as in a), closed symbols denote the adsorption, open symbols indicate the desorption branch). Exemplary SEM images of TbBTC (e) and $Eu_{0.04}Tb_{0.96}BTC$ (f) highlighting the roundish shape of the particles. Scale bar 1 µm.

Luminescent properties of $Eu_xTb_{(1-x)}BTC$ MOFs

The luminescence spectra of the samples were measured in the solid state and as a suspension in EtOH. In the solid state, upon excitation at λ_{ex} = 254 nm the pure TbBTC shows the characteristic emissions centered at approx. 489 ($^5D_4 \rightarrow {}^7F_6$), 545 ($^5D_4 \rightarrow {}^7F_5$), 586 ($^5D_4 \rightarrow {}^7F_4$) and 622 nm ($^5D_4 \rightarrow {}^7F_3$). With decreasing Tb content in the $Eu_xTb_{(1-x)}BTC$ series, the intensity of those lines decreases, while the intensity of the lines characteristic for Eu centered emissions at 595 ($^5D_0 \rightarrow {}^7F_1$), 616 ($^5D_0 \rightarrow {}^7F_2$), 653 ($^5D_0 \rightarrow {}^7F_3$) and 695 nm ($^5D_0 \rightarrow {}^7F_4$),[28] increase for low Eu ratios and decrease for higher Eu ratios. We note that, as soon as Eu is added, the Tb emission decreases and vanishes almost completely from an Eu content of 25 % onwards. Such a decrease of the Tb emission intensity upon doping the framework

with Eu has also been observed in e.g. series of $[Tb_{2x}Eu_{2-2x}(bdc)_3(H_2O)_4]_\infty$ or Eu_xTb_{1-x}DMBDC MOFs,[29,30] and has been attributed to an efficient, most likely Förster type, energy transfer from Tb to Eu.[31–33] The decrease in Eu emission with increasing Eu content might be attributed to concertation quenching in form of energy migration from Eu^{3+} to a non-radiative recombination site or by cross relaxation with other (excited) Eu sites.[30] As the excitation mainly occurs on the ligand, the energy transfer thus also involve excited states of the linker. The excited states energy of the BTC linker is higher than the $^5D_4$ (Tb) and $^5D_1$ (Eu) energetic levels. We supposed that similarly to literature reports, energy transfer occurs via intersystem crossing from linker based triplet states to $^5D_1$ level, internal conversion into $^4D_0$ energy level occurred, followed by emission into ^7F_J levels.[34]

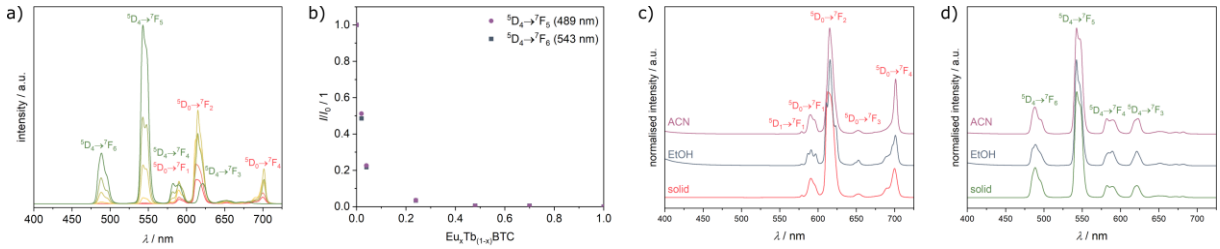

Figure 2. a) Photoluminescence spectra of $Eu_xTb_{(1-x)}$BTC MOFs [x = 0.0 to 1.0] in the solid state (λ_{ex}: 254 nm), b) corresponding quenching ratio of the Tb emission at 489 nm (purple) and 543 nm (dark gray). Comparison of solid state photoluminescence spectra with PL spectra suspension in ethanol and acetonitrile of (c) EuBTC and (d) TbBTC (λ_{ex} (suspension): 300 nm).

The emission spectra of suspension of the pure MOFs in ethanol are very similar to the PL spectra in the solid state (Figure 2), with however a slight shift of the emission wavelength of the Eu $^5D_0 \rightarrow {}^7F_2$ transition. Interestingly, when replacing ethanol with acetonitrile, the emission profile of TbBTC remains unaltered, while the emission profile of EuBTC is hugely affected. Beside the shift of the $^5D_0 \rightarrow {}^7F_2$ transition, also the relative intensities of the transitions changes as compared to the PL spectra recorded in ethanol and in the dry solid state. The luminescence intensity of the pure MOFs when dispersed in ethanol increases when rising the temperature from 293 K to 323 K (Figure 3). For EuBTC an increase of approx. 50 % is observed, independently of the transition studied. However when

TbBTC is dispersed in EtOH, the increase in luminescence intensity depends on the transition observed. While for the $^5D_4 \rightarrow {}^7F_6$ (488 nm) and $^5D_4 \rightarrow {}^7F_5$ (545 nm) transition, the increase is about 25%, it increases up to 62 % for the $^5D_4 \rightarrow {}^7F_3$ transition.

Inspired by those data, the photoluminescence properties of the $Eu_{0.02}Tb_{0.98}BTC$ and $Eu_{0.04}Tb_{0.96}BTC$ MOFs were investigated in more detail in order to use them as potential luminescent thermometers.

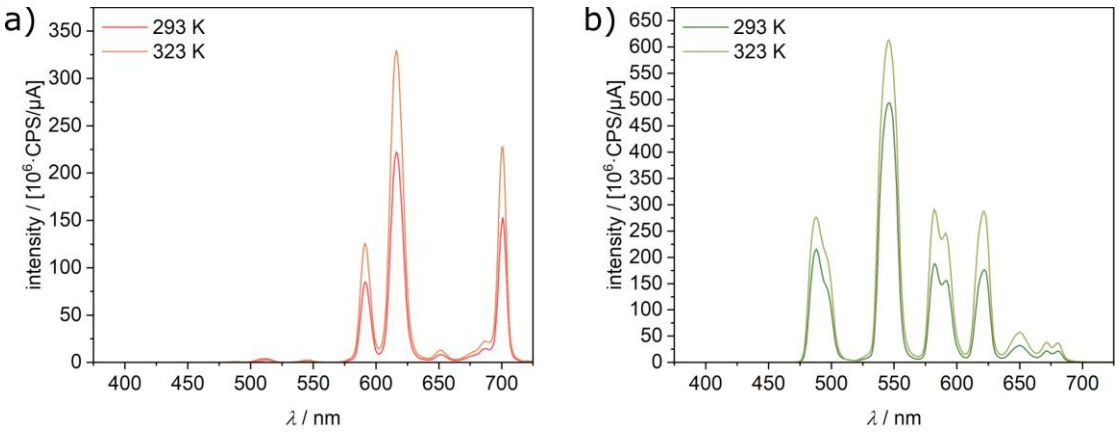

Figure 3. Photoluminescence spectra of EuBTC (a) and TbBTC (b) measured as suspension in EtOH at 293 K and at 323 K (λ_{ex}: 254 nm).

Temperature-dependent luminescence spectra were recorded for $Eu_{0.04}Tb_{0.96}BTC$ and $Eu_{0.02}Tb_{0.98}BTC$ in the temperature range from 200 to 330 K in the solid state. The terbium-based emission, e.g. at 488 nm and 542 nm, decreases linearly with increasing temperature. We note that there seems to be a discontinuity between 280 and 300 K. However, for the Eu-based emission, the temperature dependency is more complex. Between 200 and 270 K, the emission decreases linearly with increasing temperature, while above 270 K it increases again. Between 280 and 300 K also for the Eu-based emissions there is a discontinuity observed. In the range from 200 to 270 K the decrease in emission is stronger for Tb than for Eu-based emission, for both materials and in line with results on single lanthanide $Ln_2(Hpcpa)_3(H_2O)_5{\cdot}H_2O$ (H_3pcpa = *N*-(4-carboxyphenyl)oxamic acid).[28] For EuBTC doped with $CsPbBr_3$ quantum dots,[21] as well as $Eu_{0.37}Tb_{0.63}BTC$[12] an increase in emission with increasing

temperature above 293 K has been reported. In contrast for a series of $Eu_xTb_{(1-x)}$-DMBDC (x = 0.0011, 0.0046, 0.0069; DMBDC = 2,5-dimethoxy-1,4-benzenedicarboxylate) a different behaviour has been reported.[33] While Tb emission still decreases with increasing temperature, Eu emission increases with increasing temperature in the range from 10 to 300 K. Interestingly for pure Eu-DMBDC and pure Tb-

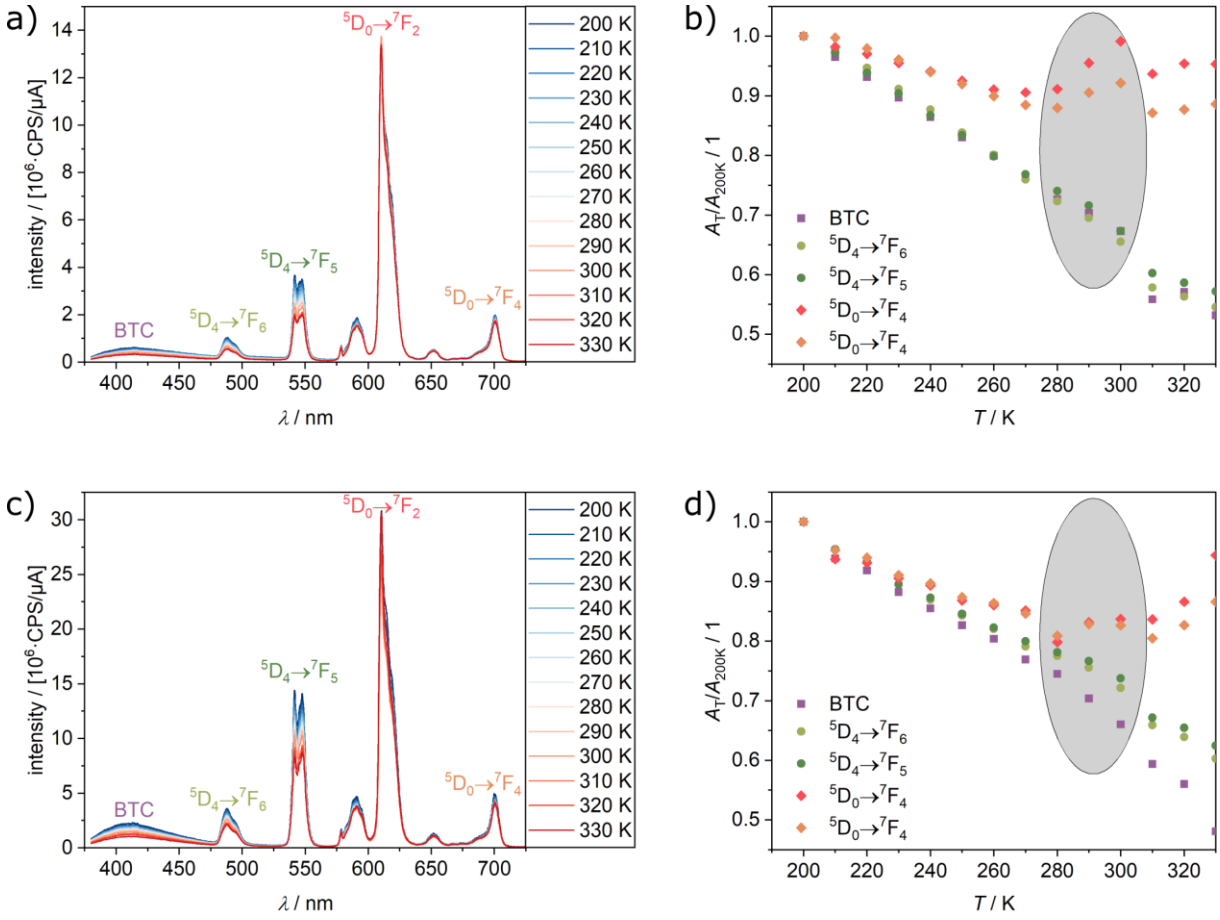

Figure 4. Temperature dependent luminescence spectra recoded between 200 and 330 K after excitation at 370 nm of $Eu_{0.04}Tb_{0.96}$BTC (a) and $Eu_{0.02}Tb_{0.98}$BTC (c). Corresponding Evolution of the luminescence, expressed as area at a given temperature divided by the area at 200 K, with temperature for $Eu_{0.04}Tb_{0.96}$BTC (b) and $Eu_{0.02}Tb_{0.98}$BTC (d). Gray circles highlight the region of discontinuity in the temperature dependency.

DMBDC, a decrease of the emission with increasing temperature has been reported. The inversion of the temperature dependency of Eu emission when doped into Tb-DMBDC matrix has been explained by an efficient energy transfer from Tb to Eu. The efficiency of this energy transfer increased with

temperature and with decreasing amount of Eu.[33] The difference to the observed profile of $Eu_{0.04}Tb_{0.96}$BTC as well as $Eu_{0.02}Tb_{0.98}$BTC might be the higher amount of Eu used in our study, making the energy transfer per Eu atom less efficient as compared to the $Eu_{0.0069}Tb_{0.9931}$-DMBDC system, in particular at low temperatures. As the efficiency of the energy transfer will most likely also increase with temperature in the $Eu_{0.04}Tb_{0.96}$BTC and $Eu_{0.02}Tb_{0.98}$BTC systems, this might explain the increase in Eu emission above 270 K. In case of $Eu_{0.02}Tb_{0.98}$BTC the lifetime of the Eu $^5D_0 \rightarrow {}^7F_2$ transition is almost constant in the entire temperature range investigated, while the lifetime of the Tb $^5D_4 \rightarrow {}^7F_5$ transition decreases with increasing temperature (Figure 5). The long rise time of the decay line of Eu $^5D_0 \rightarrow {}^7F_2$ transition might also hint to an energy transfer between the two luminescent centers.

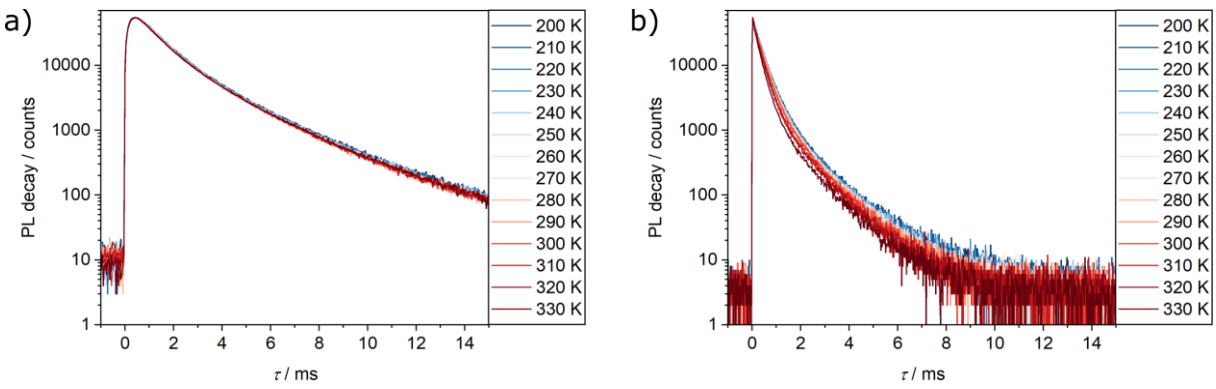

Figure 5. Photoluminescence decay curves as a function of temperature recorded on (a) the Eu $^5D_0 \rightarrow {}^7F_2$ transition and (b) the Tb $^5D_4 \rightarrow {}^7F_5$ transition.

Conclusions

Using the acetate mediated synthesis s protocol of LnBTCs, we obtained a series of $Eu_xTb_{(1-x)}$BTC MOFs, in which the ratio of the two lanthanides is controlled by the synthesis gel composition. The precise control of the lanthanide stoichiometry allows to control the luminescent properties of the final material. While for Eu loadings above 25 mol% the Tb emission is completely quenched, in $Eu_{0.04}Tb_{0.96}$BTC still remain 20% of the Tb intensity of the parent TbBTC, sufficient to be used as a rational temperature sensor. $Eu_{0.04}Tb_{0.96}$BTC and $Eu_{0.02}Tb_{0.98}$BTC, allow for rational temperature sensing in the range between 200 and 270 K and above 300 K. Interestingly, the emission profiles of

Tb centres are not affected when the material is dispersed in different solvents, while for Eu centres the emission wavelengths of the transitions as well as the intensity ratios for the different transitions changes in the presence of ethanol and acetonitrile. Therefore the solvation of the MOFs should be considered when using them as rational temperature sensors in suspensions. As only the Eu emission is affected, this solvation dependency can be rationalised and taken into account in such sensors.

AUTHOR INFORMATION

Corresponding Author

* martin.hartmann@fau.de

Author Contributions

The manuscript was written through contributions of all authors. All authors have given approval to the final version of the manuscript. ‡ These authors contributed equally.

Acknowledgements

Financial support of this work by the Deutsche Forschungsgemeinschaft (DFG, German Research Foundation), project-ID 416229255–SFB 1411 is gratefully acknowledged.

References

(1) Wang, J.-X.; Yin, J.; Shekhah, O.; Bakr, O. M.; Eddaoudi, M.; Mohammed, O. F. Energy Transfer in Metal-Organic Frameworks for Fluorescence Sensing. *ACS applied materials & interfaces* **2022**, *14* (8), 9970–9986. DOI: 10.1021/acsami.1c24759. Published Online: Feb. 17, 2022.

(2) Griffin, S. L.; Champness, N. R. A periodic table of metal-organic frameworks. *Coordination Chemistry Reviews* **2020**, *414*, 213295. DOI: 10.1016/j.ccr.2020.213295.

(3) Müller, P.; Wisser, F. M.; Bon, V.; Grünker, R.; Senkovska, I.; Kaskel, S. Postsynthetic Paddle-Wheel Cross-Linking and Functionalization of 1,3-Phenylenebis(azanetriyl)tetrabenzoate-Based MOFs. *Chem. Mater.* **2015**, *27* (7), 2460–2467. DOI: 10.1021/cm5045732.

(4) Wang, J.; Wang, J.; Li, Y.; Jiang, M.; Zhang, L.; Wu, P. A europium(iii)-based metal–organic framework as a naked-eye and fast response luminescence sensor for acetone and ferric iron. *New J. Chem.* **2016**, *40* (10), 8600–8606. DOI: 10.1039/C6NJ02163H.

(5) Müller, P.; Wisser, F. M.; Freund, P.; Bon, V.; Senkovska, I.; Kaskel, S. Optical Sensors Using Solvatochromic Metal-Organic Frameworks. *Inorg. Chem.* **2017**, *56* (22), 14164–14169. DOI: 10.1021/acs.inorgchem.7b02241. Published Online: Nov. 7, 2017.

(6) Freund, P.; Mielewczyk, L.; Rauche, M.; Senkovska, I.; Ehrling, S.; Brunner, E.; Kaskel, S. MIL-53(Al)/Carbon Films for CO 2 -Sensing at High Pressure. *ACS Sustainable Chem. Eng.* **2019**, *7* (4), 4012–4018. DOI: 10.1021/acssuschemeng.8b05368.

(7) Freund, P.; Senkovska, I.; Kaskel, S. Switchable Conductive MOF-Nanocarbon Composite Coatings as Threshold Sensing Architectures. *ACS applied materials & interfaces* **2017**, *9* (50), 43782–43789. DOI: 10.1021/acsami.7b13924. Published Online: Dec. 7, 2017.

(8) Roy, S.; Chakraborty, A.; Maji, T. K. Lanthanide–organic frameworks for gas storage and as magneto-luminescent materials. *Coordination Chemistry Reviews* **2014**, *273-274*, 139–164. DOI: 10.1016/j.ccr.2014.03.035.

(9) Xu, H.; Cao, C.-S.; Kang, X.-M.; Zhao, B. Lanthanide-based metal-organic frameworks as luminescent probes. *Dalton transactions (Cambridge, England : 2003)* **2016**, *45* (45), 18003–18017. DOI: 10.1039/c6dt02213h.

(10) Lucena, M. A. M.; Oliveira, M. F. L.; Arouca, A. M.; Talhavini, M.; Ferreira, E. A.; Alves, S.; Veiga-Souza, F. H.; Weber, I. T. Application of the Metal-Organic Framework Eu(BTC) as a Luminescent Marker for Gunshot Residues: A Synthesis, Characterization, and Toxicity Study. *ACS*

applied materials & interfaces **2017**, *9* (5), 4684–4691. DOI: 10.1021/acsami.6b13474. Published Online: Jan. 25, 2017.

(11) Xie, Y.; Sun, G.; Mandl, G. A.; Maurizio, S. L.; Chen, J.; Capobianco, J. A.; Sun, L. Upconversion Luminescence through Cooperative and Energy-Transfer Mechanisms in Yb3+ -Metal-Organic Frameworks. *Angewandte Chemie (International ed. in English)* **2023**, *62* (4), e202216269. DOI: 10.1002/anie.202216269. Published Online: Dec. 19, 2022.

(12) Wang, H.; Zhao, D.; Cui, Y.; Yang, Y.; Qian, G. A Eu/Tb-mixed MOF for luminescent high-temperature sensing. *Journal of Solid State Chemistry* **2017**, *246*, 341–345. DOI: 10.1016/j.jssc.2016.12.003.

(13) Yang, W.; Feng, J.; Song, S.; Zhang, H. Microwave-assisted modular fabrication of nanoscale luminescent metal-organic framework for molecular sensing. *Chemphyschem : a European journal of chemical physics and physical chemistry* **2012**, *13* (11), 2734–2738. DOI: 10.1002/cphc.201200265. Published Online: Jun. 15, 2012.

(14) Chen, B.; Yang, Y.; Zapata, F.; Lin, G.; Qian, G.; Lobkovsky, E. B. Luminescent Open Metal Sites within a Metal–Organic Framework for Sensing Small Molecules. *Adv. Mater.* **2007**, *19* (13), 1693–1696. DOI: 10.1002/adma.200601838.

(15) Xiao, Y.; Wang, L.; Cui, Y.; Chen, B.; Zapata, F.; Qian, G. Molecular sensing with lanthanide luminescence in a 3D porous metal-organic framework. *Journal of Alloys and Compounds* **2009**, *484* (1-2), 601–604. DOI: 10.1016/j.jallcom.2009.05.004.

(16) Jiang, H.-L.; Tsumori, N.; Xu, Q. A series of (6,6)-connected porous lanthanide−organic framework enantiomers with high thermostability and exposed metal sites: scalable syntheses, structures, and sorption properties. *Inorg. Chem.* **2010**, *49* (21), 10001–10006. DOI: 10.1021/ic101294s.

(17) Yao, Q.; Bermejo Gómez, A.; Su, J.; Pascanu, V.; Yun, Y.; Zheng, H.; Chen, H.; Liu, L.; Abdelhamid, H. N.; Martín-Matute, B.; Zou, X. Series of Highly Stable Isoreticular Lanthanide Metal–Organic Frameworks with Expanding Pore Size and Tunable Luminescent Properties. *Chem. Mater.* **2015**, *27* (15), 5332–5339. DOI: 10.1021/acs.chemmater.5b01711.

(18) Pal, S.; Bhunia, A.; Jana, P. P.; Dey, S.; Möllmer, J.; Janiak, C.; Nayek, H. P. Microporous La-metal-organic framework (MOF) with large surface area. *Chemistry (Weinheim an der Bergstrasse, Germany)* **2015**, *21* (7), 2789–2792. DOI: 10.1002/chem.201405168. Published Online: Dec. 17, 2014.

(19) Guo, H.; Zhu, Y.; Qiu, S.; Lercher, J. A.; Zhang, H. Coordination Modulation Induced Synthesis of Nanoscale Eu1-xTbx-Metal-Organic Frameworks for Luminescent Thin Films. *Adv. Mater.* **2010**, *22* (37), 4190–4192. DOI: 10.1002/adma.201000844.

(20) Lian, X.; Yan, B. A lanthanide metal–organic framework (MOF-76) for adsorbing dyes and fluorescence detecting aromatic pollutants. *RSC Adv.* **2016**, *6* (14), 11570–11576. DOI: 10.1039/C5RA23681A.

(21) Liu, J.; Zhao, Y.; Li, X.; Wu, J.; Han, Y.; Zhang, X.; Xu, Y. Dual-Emissive CsPbBr 3 @Eu-BTC Composite for Self-Calibrating Temperature Sensing Application. *Crystal Growth & Design* **2020**, *20* (1), 454–459. DOI: 10.1021/acs.cgd.9b01374.

(22) Brunckova, H.; Mudra, E.; Rocha, L.; Nassar, E.; Nascimento, W.; Kolev, H.; Kovalcikova, A.; Molcanova, Z.; Podobova, M.; Medvecky, L. Preparation and characterization of isostructural lanthanide Eu/Gd/Tb metal-organic framework thin films for luminescent applications. *Applied Surface Science* **2021**, *542*, 148731. DOI: 10.1016/j.apsusc.2020.148731.

(23) Duan, T.-W.; Yan, B. Hybrids based on lanthanide ions activated yttrium metal–organic frameworks: functional assembly, polymer film preparation and luminescence tuning. *J. Mater. Chem. C* **2014**, *2* (26), 5098–5104. DOI: 10.1039/C4TC00414K.

(24) Xu, B.; Guo, H.; Wang, S.; Li, Y.; Zhang, H.; Liu, C. Solvothermal synthesis of luminescent Eu(BTC)(H2O)DMF hierarchical architectures. *CrystEngComm* **2012**, *14* (8), 2914. DOI: 10.1039/c2ce06572j.

(25) Rosi, N. L.; Kim, J.; Eddaoudi, M.; Chen, B.; O'Keeffe, M.; Yaghi, O. M. Rod packings and metal-organic frameworks constructed from rod-shaped secondary building units. *J. Am. Chem. Soc.* **2005**, *127* (5), 1504–1518. DOI: 10.1021/ja045123o.

(26) Rzączyńska, Z.; Ostasz, A.; Pikus, S. Thermal properties of rare earth elements complexes with 1,3,5-benzenetricarboxylic acid. *J Therm Anal Calorim* **2005**, *82* (2), 347–351. DOI: 10.1007/s10973-005-0901-5.

(27) Almáši, M.; Zeleňák, V.; Kuchár, J.; Bourrelly, S.; Llewellyn, P. L. New members of MOF-76 family containing Ho(III) and Tm(III) ions: Characterization, stability and gas adsorption properties. *Colloids and Surfaces A: Physicochemical and Engineering Aspects* **2016**, *496*, 114–124. DOI: 10.1016/j.colsurfa.2015.10.048.

(28) Oliveira Maciel, J. W. de; Lemes, M. A.; Valdo, A. K.; Rabelo, R.; Martins, F. T.; Queiroz Maia, L. J.; Santana, R. C. de; Lloret, F.; Julve, M.; Cangussu, D. Europium(III), Terbium(III), and Gadolinium(III) Oxamato-Based Coordination Polymers: Visible Luminescence and Slow Magnetic Relaxation. *Inorg. Chem.* **2021**, *60* (9), 6176–6190. DOI: 10.1021/acs.inorgchem.0c03226. Published Online: Apr. 16, 2021.

(29) Liang, C. J.; Wong, T. C.; Hung, L. S.; Lee, S. T.; Hong, Z. R.; Li, W. L. Self-quenching of excited europium ions in Eu(DBM) 3 bath-based organic electroluminescent devices. *J. Phys. D: Appl. Phys.* **2001**, *34* (12), L61-L64. DOI: 10.1088/0022-3727/34/12/102.

(30) Hansen, P.-A.; Granerød, C. S.; Prytz, Ø.; Nilsen, O. Controlling luminescence and quenching mechanisms in subnanometer multilayer structure of europium titanium oxide thin films. *J. Lumin.* **2019**, *215*, 116618. DOI: 10.1016/j.jlumin.2019.116618.

(31) Jena, H. S.; Kaczmarek, A. M.; Krishnaraj, C.; Feng, X.; Vijayvergia, K.; Yildirim, H.; Zhao, S.-N.; van Deun, R.; van Der Voort, P. White Light Emission Properties of Defect Engineered Metal–Organic Frameworks by Encapsulation of Eu 3+ and Tb 3+. *Crystal Growth & Design* **2019**, *19* (11), 6339–6350. DOI: 10.1021/acs.cgd.9b00824.

(32) Haquin, V.; Etienne, M.; Daiguebonne, C.; Freslon, S.; Calvez, G.; Bernot, K.; Le Pollès, L.; Ashbrook, S. E.; Mitchell, M. R.; Bünzli, J.-C.; Eliseeva, S. V.; Guillou, O. Color and Brightness Tuning in Heteronuclear Lanthanide Terephthalate Coordination Polymers. *Eur. J. Inorg. Chem.* **2013**, *2013* (20), 3464–3476. DOI: 10.1002/ejic.201300381.

(33) Cui, Y.; Xu, H.; Yue, Y.; Guo, Z.; Yu, J.; Chen, Z.; Gao, J.; Yang, Y.; Qian, G.; Chen, B. A luminescent mixed-lanthanide metal-organic framework thermometer. *J. Am. Chem. Soc.* **2012**, *134* (9), 3979–3982. DOI: 10.1021/ja2108036. Published Online: Feb. 24, 2012.

(34) Nosov, V. G.; Kupryakov, A. S.; Kolesnikov, I. E.; Vidyakina, A. A.; Tumkin, I. I.; Kolesnik, S. S.; Ryazantsev, M. N.; Bogachev, N. A.; Skripkin, M. Y.; Mereshchenko, A. S. Heterometallic Europium(III)-Lutetium(III) Terephthalates as Bright Luminescent Antenna MOFs. *Molecules (Basel, Switzerland)* **2022**, *27* (18). DOI: 10.3390/molecules27185763. Published Online: Sep. 6, 2022.